Advances in Computational Mathematics (2019) 45:1551–1580
https://doi.org/10.1007/s10444-019-09678-w

Efficient numerical schemes with unconditional energy stabilities for the modified phase field crystal equation

Qi Li[1] · Liquan Mei[1] · Xiaofeng Yang[2] · Yibao Li[1]

Received: 28 August 2018 / Accepted: 20 February 2019 /
Published online: 2 March 2019

Abstract

We consider numerical approximations for the modified phase field crystal equation in this paper. The model is a nonlinear damped wave equation that includes both diffusive dynamics and elastic interactions. To develop easy-to-implement time-stepping schemes with unconditional energy stabilities, we adopt the "Invariant Energy Quadratization" approach. By using the first-order backward Euler, the second-order Crank–Nicolson, and the second-order BDF2 formulas, we obtain three linear and symmetric positive definite schemes. We rigorously prove their unconditional energy stabilities and implement a number of 2D and 3D numerical experiments to demonstrate the accuracy, stability, and efficiency.

Keywords Modified phase field crystal equation · Unconditionally energy stable · Pseudo energy · Invariant energy quadratization

Communicated by: Carlos Garcia-Cervera

✉ Liquan Mei
lqmei@mail.xjtu.edu.cn

Qi Li
liqihao2000@126.com

Xiaofeng Yang
xfyang@math.sc.edu.cn

Yibao Li
yibaoli@xjtu.edu.cn

[1] School of Mathematics and Statistics, Xi'an Jiaotong University, Xi'an 710049, Shaanxi, People's Republic of China

[2] Department of Mathematics, University of South Carolina, Columbia, SC 29208, USA

1 Introduction

The phase field crystal (PFC) equation was proposed by Elder and Grant in [8, 9] as a continuum model of crystalline phase to study the dynamics of atomic-scale crystal growth on diffusive time scales. An order parameter (phase field variable) that represents the concentration field of a coarse-grained temporal average of the density of atoms is introduced to describe the phase transition from the liquid phase to the crystal phase. More precisely, the density is relatively homogeneous in the liquid phase and spatially periodic (i.e., crystalline) in the solid phase. Thus, a free energy is postulated to generate the periodic structure of a crystal lattice, by incorporating a specific form of the spatial gradients. The equation has been used to study various phenomena, including elastic and plastic deformations, grain growth, dendritic and eutectic solidification, and epitaxial growth [10, 19].

The PFC equation evolves only on diffusive time scales; thus, it does not contain a mechanism for simulating elastic interactions, for example, the deformation properties of noncrystalline solids. In order to overcome this problem, Stefanovic et al. [22, 23] introduced the modified phase field crystal (MPFC) equation that includes both diffusive dynamics and elastic interactions. The MPFC equation is a sixth-order nonlinear damped wave equation modeling a viscoelastic response to perturbations to the density field. In this equation, perturbations in the density field are transmitted by waves that travel essentially undamped up to a certain length scale determined by the parameters. When this length scale is of the order of the size of the system, a separation of elastic relaxation and diffusion time scales may be practically observed [22]. Since the MPFC equation adds a wave operator for elastic interaction on the basis of PFC equation, compared with the PFC equation, the MPFC equation has a more complicated form which brings more difficulties in developing time-marching schemes.

There have been a few works on the numerical approximation for the MPFC equation. Stefanovic et al., [23] employed a semi-implicit finite difference scheme with a multigrid algorithm for solving the algebraic equations. They did not give any relevant numerical analysis about unique solvability and energy stability. Wang and Wise [25] proposed a first-order energy stable convex splitting nonlinear scheme for the MPFC equation. Subsequently, a second-order energy stable convex splitting scheme was presented by Baskaran et al. in [1, 2]. Lee et al. [17] proposed first- and second-order energy stable schemes based on a new convex splitting of energy functional for the MPFC equation. Dehghan and Mohammadi [7] used a semi-implicit method for the PFC and MPFC equations, which split the linear terms into backward and forward pieces while treating the nonlinear term explicitly. Grasselli and Pierre [15] proposed an energy stable and convergent finite element scheme for the MPFC equation, and their time discretization can be seen as a Crank–Nicolson scheme with a second-order stabilization term. Guo and Xu [16] developed first- and second-order energy stable schemes with adaptive time-stepping strategy for the MPFC equation.

Although there had been quite a few schemes developed for the MPFC equation, it is worth noting that almost all those schemes were based on convex splitting approach and thus nonlinear. Hence, the implementations are often complicated and the computational costs are high. To obtain linear schemes for this model, the main difficulty

is on how to discretize the quartic potential. One solution is to use the so-called linear stabilization approach [20, 26] that can introduce purely linear schemes and is therefore easy to implement. Its stability, however, usually requires a special property (generalized maximum principle) [20, 21] satisfied by the classical PDE solution and the numerical solution, which is very hard to prove in general.

The main purpose of this paper is to construct linear time-marching schemes with unconditional energy stabilities, namely, the schemes preserve the thermodynamically consistent dissipation law (energy stable) at the discrete level without any constraints on the time step size. This goal is achieved by adopting the "Invariant Energy Quadratization" (IEQ) approach (cf. [4–6, 12–14, 18, 27–34]). We propose three time discretization schemes based on the first-order backward Euler, the second-order Crank–Nicolson, and the second-order BDF2, respectively. We further show that these schemes satisfy modified energy laws and therefore unconditionally energy stable. Moreover, at each time step, the schemes lead to a symmetric positive definite linear system and one can always solve it using the well-developed fast matrix solvers efficiently.

The paper is organized as follows. In Section 2, the governing equation and corresponding energy law are presented in the continuous case. In Section 3, we propose three numerical schemes and prove the unconditional energy stability and the well-posedness of the linear systems in the time semi-discrete case. The fully discrete schemes and algorithm implementation are presented in Section 4. In Section 5, various numerical experiments in 2D and 3D are carried out to illustrate the accuracy, energy stability, and efficiency of the proposed schemes. Finally, some concluding remarks are given in Section 6.

2 Governing systems

Before introducing the governing equation, we first fix some notations that will be used later. For each $s \geq 0$, let $(\cdot,\cdot)_s$ and $\|\cdot\|_s$ be the $H^s(\Omega)$ inner product and norm, respectively. Note that $H^0(\Omega) = L^2(\Omega)$. In particular, we use $(\cdot,\cdot)$ and $\|\cdot\|$ to denote the L^2 inner product $(\cdot,\cdot)_0$ and norm $\|\cdot\|_0$, respectively. We define Sobolev spaces $L_0^2(\Omega) = \{v \in L^2(\Omega) \mid (v,1) = 0\}$, $L_{per}^2(\Omega) = \{v \in L^2(\Omega) \mid v \text{ is periodic on } \partial\Omega\}$, $H_{per}^s(\Omega) = \{v \in H^s(\Omega) \mid v \text{ is periodic on } \partial\Omega\}$, and denote by $H_{per}^{-s}(\Omega)$ the dual space of $H_{per}^s(\Omega)$.

We consider a free energy functional of Swift–Hohenberg type [8, 9, 24]

$$E(\phi) = \int_\Omega \left(\frac{1}{4}\phi^4 + \frac{1}{2}\phi\,(1+\Delta)^2\,\phi - \frac{\epsilon}{2}\phi^2 \right) dx, \tag{2.1}$$

where Ω is a domain in $\mathbb{R}^d$ $(d = 1, 2, 3)$, ϕ is the atomic density field, and $0 < \epsilon < 1$ is a positive constant with physical significance. Then the modified phase field crystal (MPFC) equation is the pseudo-gradient flow

$$\phi_{tt} + \beta\phi_t = M\Delta\mu, \tag{2.2}$$

where $\beta > 0$ is a constant, $M > 0$ is a constant mobility and μ is the chemical potential defined as

$$\mu := \frac{\delta E}{\delta \phi} = \phi^3 + (1+\Delta)^2\phi - \epsilon\phi, \tag{2.3}$$

and $\frac{\delta E}{\delta \phi}$ denotes the variational derivative of E with respect to ϕ. We assume all variables are periodic on $\partial\Omega$, that is, the values of variables on the opposite facets of a hypercube $\Omega \subset \mathbb{R}^d$ $(d = 1, 2, 3)$ are identified. The analysis is also true for physical boundary conditions like Neumann type, or any other type of boundary conditions which do not involve any boundary integrals in the variational formulation of the equation. We use periodic boundary condition since that is used in most analytical/numerical works of MPFC equation.

The mass conservation will hold provided the initial condition satisfying $\int_\Omega \phi_t(x,0)\,dx = 0$. To see this, by integrating (2.2) over Ω with the periodic boundary condition for μ, we obtain

$$\frac{d}{dt}\int_\Omega \phi_t(x,t)\,dx + \beta\int_\Omega \phi_t(x,t)\,dx = M\int_{\partial\Omega} \nabla\mu\cdot n\,ds = 0, \tag{2.4}$$

where n is the unit outward normal on the boundary $\partial\Omega$. (2.4) is actually an ODE system for time, and its solution is

$$\int_\Omega \phi_t(x,t)\,dx = e^{-\beta t}\int_\Omega \phi_t(x,0)\,dx. \tag{2.5}$$

Thus, if the initial condition satisfies $\int_\Omega \phi_t(x,0)\,dx = 0$, we obtain the mass conservation

$$\int_\Omega \phi_t(x,t)\,dx = \int_\Omega \phi_{tt}(x,t)\,dx = 0. \tag{2.6}$$

We now derive the energy dissipation law for MPFC model (2.2) and (2.3), for which the inverse Laplace operator $(-\Delta)^{-1}$ and H^{-1}_{per} inner product are needed. Suppose $f \in L^2_0(\Omega)$, we define $v_f \in H^2_{per}(\Omega)\cap L^2_0(\Omega)$ to be the unique solution to the periodic boundary value problem

$$-\Delta v_f = f \text{ in } \Omega. \tag{2.7}$$

In this case, we define $v_f := (-\Delta)^{-1} f$. Suppose that $f, g \in L^2_0(\Omega)$, then we define H^{-1}_{per} inner product and norm

$$(f,g)_{-1} := (\nabla v_f, \nabla v_g), \quad \|f\|_{-1} := \sqrt{(f,f)_{-1}}. \tag{2.8}$$

Note that, via integration by parts, we have the following identity

$$(f,g)_{-1} = \left((-\Delta)^{-1} f, g\right) = \left((-\Delta)^{-1} g, f\right) = (g,f)_{-1}. \tag{2.9}$$

We introduce a new variable $\psi = \phi_t$. Since $\int_\Omega \psi\,dx = \int_\Omega \psi_t\,dx = 0$, i.e., $\psi \in L^2_0(\Omega)$ and $\psi_t \in L^2_0(\Omega)$, using the operator Δ^{-1}, we rewrite the system (2.2) and (2.3) as follows,

$$\Delta^{-1}\psi_t + \beta\Delta^{-1}\psi = M\left(\phi^3 + (1+\Delta)^2\phi - \epsilon\phi\right). \tag{2.10}$$

By taking the L^2 inner product of (2.10) with $\frac{1}{M}\phi_t$, we obtain the following energy dissipation law

$$\frac{d}{dt}\mathcal{E}(\phi,\psi) = -\frac{\beta}{M}\|\psi\|_{-1}^2 \le 0, \tag{2.11}$$

where the pseudo energy $\mathcal{E}(\phi,\psi)$ is defined as

$$\mathcal{E}(\phi,\psi) := E(\phi) + \frac{1}{2M}\|\psi\|_{-1}^2. \tag{2.12}$$

This means that the pseudo energy $\mathcal{E}(\phi,\psi)$ of the system (2.2) and (2.3) decays in time.

Remark 1 Note that in [3, 11, 25], the MPFC equation is written in another version, namely,

$$\tilde{\beta}\phi_{tt} + \phi_t = M\Delta\mu, \quad \tilde{\beta} > 0, \tag{2.13}$$

which expresses the model as a perturbed parabolic equation. In this paper, we focus on the version (2.2), but all numerical schemes and analysis can be also true for the version (2.13).

3 Numerical schemes

In this section, we develop a set of time-marching schemes to solve the system (2.2)–(2.3) by using the IEQ approach. Its essential idea is to transform the nonlinear potential into a simple quadratic form in terms of some new variables. Such simple way of quadratization has the following advantages: (i) the complicated nonlinear potential is transferred to quadratic polynomial form that is much easier to handle; (ii) the derivative of the quadratic polynomial is linear, which provides the fundamental support for linearization method; (iii) the quadratic formulation in terms of new variables can automatically preserve the positivity (or boundedness from below) of the nonlinear potentials [29, 32]. To this end, we introduce two auxiliary functions as follows,

$$p = \Delta^{-1}\psi, \quad U = \sqrt{F(\phi)+B}, \tag{3.1}$$

where $F(\phi) = \frac{1}{4}\phi^4 - \frac{\epsilon}{2}\phi^2$ is a nonlinear potential, and B is a positive constant to ensure $F(\phi) + B > 0$, $\forall\phi \in \mathbb{R}$. In turn, the free energy functional (2.1) can be rewritten as

$$\hat{E}(\phi,U) = \int_\Omega \left(U^2 + \frac{1}{2}\phi\left(1+\Delta\right)^2\phi - B\right)dx, \tag{3.2}$$

and the pseudo energy (2.12) becomes

$$\hat{\mathcal{E}}(\phi,U,p) = \hat{E}(\phi,U) + \frac{1}{2M}\|\nabla p\|^2. \tag{3.3}$$

Now, we have a new but equivalent PDE system as follows:

$$\psi_t + \beta\psi = M\Delta\mu, \tag{3.4a}$$
$$\mu = H(\phi)U + (1+\Delta)^2\phi, \tag{3.4b}$$
$$\psi = \phi_t, \tag{3.4c}$$
$$U_t = \frac{1}{2}H(\phi)\phi_t, \tag{3.4d}$$

where

$$H(\phi) = \frac{f(\phi)}{\sqrt{F(\phi)+B}}, \quad f(\phi) = F'(\phi). \tag{3.4e}$$

(3.4d) is an ODE system for time; thus, U does not need any boundary conditions. Therefore, the system (3.4a)–(3.4d) form a closed PDE system for the variables ϕ, μ, ψ, and U with the periodic boundary conditions and the following compatible initial conditions,

$$\phi|_{(t=0)} = \phi^0, \quad \psi|_{(t=0)} = 0, \quad U|_{(t=0)} = \sqrt{F(\phi^0)+B}, \tag{3.5}$$

where we simply set the initial profile of ψ to be zero point-wise.

The new system (3.4) in terms of the new variables still follows an energy dissipative law. By applying the inverse Laplace operator Δ^{-1} to (3.4a), taking the L^2 inner product of it with $\frac{\phi_t}{M}$, of (3.4b) with ϕ_t, using (3.4c) and (3.4d), and summing them up, we can obtain the following energy dissipation law of the new system (3.4) as

$$\frac{d}{dt}\hat{\mathcal{E}}(\phi, U, p) = -\frac{\beta}{M}\|\nabla p\|^2 \le 0. \tag{3.6}$$

Remark 2 We note that the transformed system (3.4) is equivalent with the original system (2.2)–(2.3). The energy (3.3) and its dissipation law (3.6) for the transformed system are equivalent with the original energy (2.12) and dissipation law (2.11). Therefore, in the following sections, we will propose numerical approximation for the transformed system (3.4) and show the numerical schemes preserve the properties of mass conservation and energy dissipations, accordingly.

Remark 3 For the nonlinear potential $F(\phi) = \frac{1}{4}\phi^4 - \frac{\epsilon}{2}\phi^2$, by taking $B = \frac{\epsilon^2}{4}$, we can obtain $f(\phi) = \phi^3 - \epsilon\phi$, $U = \frac{1}{2}(\phi^2 - \epsilon)$ and $H(\phi) = 2\phi$.

We now develop time-marching numerical schemes to solve the new system (3.4). The proof of the unconditional energy stability of the schemes follows the similar lines as in the derivation of the energy law (3.6). Let $\delta t > 0$ denote the time step size and set $t^n = n\delta t$ for $0 \le n \le N_T$ with the final time $T = N_T\delta t$, and u^n denote the numerical approximation of $u(t^n)$.

3.1 The first-order scheme

We first develop a first-order scheme derived by the backward Euler method.

Scheme 1 Assuming that (ϕ^n, ψ^n, U^n) are already calculated with $n \geq 0$, we then update $(\phi^{n+1}, \psi^{n+1}, U^{n+1})$ as follows,

$$\frac{\psi^{n+1}-\psi^n}{\delta t} + \beta\psi^{n+1} = M\Delta\mu^{n+1}, \tag{3.7a}$$

$$\mu^{n+1} = H(\phi^n)U^{n+1} + (1+\Delta)^2\phi^{n+1}, \tag{3.7b}$$

$$\psi^{n+1} = \frac{\phi^{n+1}-\phi^n}{\delta t}, \tag{3.7c}$$

$$U^{n+1} - U^n = \frac{1}{2}H(\phi^n)(\phi^{n+1}-\phi^n), \tag{3.7d}$$

where

$$H(\phi^n) = \frac{f(\phi^n)}{\sqrt{F(\phi^n)+B}}. \tag{3.8}$$

Since the nonlinear coefficient $H(\phi)$ of the new variable U is treated explicitly, we can rewrite the equations (3.7c) and (3.7d) as follows:

$$\begin{cases} U^{n+1} = \dfrac{1}{2}H(\phi^n)\phi^{n+1} + g_1^n, & (3.9) \\ \psi^{n+1} = \dfrac{1}{\delta t}\phi^{n+1} + g_2^n, & (3.10) \end{cases}$$

where $g_1^n = U^n - \frac{1}{2}H(\phi^n)\phi^n$, $g_2^n = -\frac{\phi^n}{\delta t}$. Thus (3.7a) and (3.7b) can be rewritten as the following linear system:

$$\alpha^*\phi^{n+1} = M\Delta\mu^{n+1} + g_3^n, \tag{3.11}$$

$$\mu^{n+1} = P_1(\phi^{n+1}) + g_4^n, \tag{3.12}$$

where

$$\begin{cases} \alpha^* = \left(\dfrac{1}{\delta t}+\beta\right)\dfrac{1}{\delta t}, \\ P_1(\phi^{n+1}) = \dfrac{1}{2}H(\phi^n)H(\phi^n)\phi^{n+1} + (1+\Delta)^2\phi^{n+1}, \\ g_3^n = \alpha^*\phi^n + \dfrac{1}{\delta t}\psi^n, \\ g_4^n = H(\phi^n)g_1^n. \end{cases} \tag{3.13}$$

Therefore, we can solve ϕ^{n+1} and μ^{n+1} directly from (3.11) and (3.12). Once we obtain ϕ^{n+1}, U^{n+1} and ψ^{n+1} are automatically given in (3.9)–(3.10). Furthermore, we notice

$$\big(P_1(\phi), \psi\big) = \frac{1}{2}\big(H(\phi^n)\phi, H(\phi^n)\psi\big) + \big((1+\Delta)\phi, (1+\Delta)\psi\big), \tag{3.14}$$

if ψ enjoys the same boundary condition as ϕ. Therefore, the linear operator $P_1(\cdot)$ is symmetric (self-adjoint). Moreover, for any ϕ with $\int_\Omega \phi\, dx = 0$, we have

$$\big(P_1(\phi), \phi\big) = \frac{1}{2}\|H(\phi^n)\phi\|^2 + \|(1+\Delta)\phi\|^2 \geq 0, \tag{3.15}$$

where "= " is valid if and only if $\phi \equiv 0$.

We first show the well-posedness of the linear system (3.7) (or (3.11)–(3.12)) as follows.

Theorem 1 *The linear system* (3.11)–(3.12) *is uniquely solvable, and the linear operator is symmetric positive definite.*

Proof From (3.7a), by taking the L^2 inner product with 1 and notice $\int_\Omega \psi^0\,dx = 0$, we derive

$$\left(\frac{1}{\delta t} + \beta\right)\int_\Omega \psi^{n+1}\,dx = \frac{1}{\delta t}\int_\Omega \psi^n\,dx = 0. \tag{3.16}$$

From (3.7c), we have

$$\int_\Omega \phi^{n+1}\,dx = \int_\Omega \phi^n\,dx = \cdots = \int_\Omega \phi^0\,dx. \tag{3.17}$$

Let $V_\phi = \frac{1}{|\Omega|}\int_\Omega \phi^0\,dx$, and we define

$$\widehat{\phi}^{n+1} = \phi^{n+1} - V_\phi. \tag{3.18}$$

Thus, from (3.11)–(3.12), $(\widehat{\phi}^{n+1}, \mu^{n+1})$ are the solutions for the following equations with unknowns (ϕ, w),

$$\alpha^*\phi = M\Delta w + f^n, \tag{3.19}$$

$$w = P_1(\phi) + g^n, \tag{3.20}$$

where $f^n = g_3^n - \alpha^* V_\phi$, $\int_\Omega f^n\,dx = 0$, $g^n = g_4^n$, $\int_\Omega \phi\,dx = 0$. Applying $-\Delta^{-1}$ to (3.19) and using (3.20), we obtain

$$-\alpha^*\Delta^{-1}\phi + MP_1(\phi) = -Mg^n - \Delta^{-1}f^n. \tag{3.21}$$

Let us express the above linear system (3.21) as $\mathbb{A}\phi = b$.

i. For any ϕ_1 and ϕ_2 in $H^2(\Omega)$ with the periodic boundary condition and $\int_\Omega \phi_1\,dx = \int_\Omega \phi_2\,dx = 0$, using integration by parts, we derive

$$\begin{aligned}\big(\mathbb{A}(\phi_1), \phi_2\big) =& -\alpha^*(\Delta^{-1}\phi_1, \phi_2) + M(P_1(\phi_1), \phi_2)\\ \le& C_1\Big(\|\nabla\Delta^{-1}\phi_1\|\|\nabla\Delta^{-1}\phi_2\| + \|\Delta\phi_1\|\|\Delta\phi_2\|\\ &+\|\nabla\phi_1\|\|\nabla\phi_2\| + \|\phi_1\|\|\phi_2\|\Big)\\ \le& C_2\|\phi_1\|_2\|\phi_2\|_2.\end{aligned} \tag{3.22}$$

Therefore, the bilinear form $\big(\mathbb{A}(\cdot), \cdot\big)$ is bounded.

ii. For any ϕ in $H^2(\Omega)$, it is easy to derive that,

$$\big(\mathbb{A}(\phi), \phi\big) = \alpha^*\|\phi\|_{-1}^2 + \frac{M}{2}\|H(\phi^n)\phi\|^2 + M\|(1+\Delta)\phi\|^2 \ge C_3\|\phi\|_2^2, \tag{3.23}$$

for $\int_\Omega \phi\,dx = 0$ from Poincaré's inequality. Thus, the bilinear form $\big(\mathbb{A}(\cdot), \cdot\big)$ is coercive. Here, $C_1 > 0$, $C_2 > 0$, and $C_3 > 0$ are constants.

Then, the well-posedness of the linear system $\mathbb{A}\phi = b$ in the weak sense comes from the Lax–Milgram theorem, i.e., the linear system (3.21) admits a unique weak solution in $H^2(\Omega)$.

For any ϕ_1 and ϕ_2 with $\int_\Omega \phi_1\, dx = 0$ and $\int_\Omega \phi_2\, dx = 0$, we can easily derive

$$\big(\mathbb{A}(\phi_1), \phi_2\big) = \big(\phi_1, \mathbb{A}(\phi_2)\big). \tag{3.24}$$

Thus, $\mathbb{A}$ is self-adjoint. Meanwhile, the positive definiteness of $\mathbb{A}$ follows from coercivity in (3.23). Therefore, the operator $\mathbb{A}$ is symmetric positive definite. □

Theorem 2 *The scheme* (3.7) *(or* (3.11)–(3.12)*) is unconditionally energy stable, that is, it satisfies the following discrete energy dissipation law*

$$\frac{E_{1st}^{n+1} - E_{1st}^{n}}{\delta t} \le -\frac{\beta}{M}\left\|\nabla p^{n+1}\right\|^2 \le 0, \tag{3.25}$$

where

$$E_{1st} = \|U\|^2 + \frac{1}{2}\|(1+\Delta)\phi\|^2 + \frac{1}{2M}\|\nabla p\|^2 - B|\Omega|. \tag{3.26}$$

Proof Firstly, we combine (3.7a) and (3.7b) together and apply the Δ^{-1} to obtain

$$\frac{1}{\delta t M}\Delta^{-1}\left(\psi^{n+1} - \psi^n\right) + \frac{\beta}{M}\Delta^{-1}\psi^{n+1} = H(\phi^n)U^{n+1} + (1+\Delta)^2\phi^{n+1}. \tag{3.27}$$

Secondly, by taking the L^2 inner product of (3.27) with $\phi^{n+1} - \phi^n$, and applying the following identities

$$2(a-b,a) = a^2 - b^2 + (a-b)^2, \quad 2(a-b,b) = a^2 - b^2 - (a-b)^2, \tag{3.28}$$

we obtain

$$\begin{aligned}&\frac{1}{\delta t M}\left(\Delta^{-1}\left(\psi^{n+1} - \psi^n\right), \phi^{n+1} - \phi^n\right) + \frac{\beta}{M}\left(\Delta^{-1}\psi^{n+1}, \phi^{n+1} - \phi^n\right)\\ &\quad = \left(H(\phi^n)U^{n+1}, \phi^{n+1} - \phi^n\right) + \frac{1}{2}\Big(\|(1+\Delta)\phi^{n+1}\|^2\\ &\quad -\|(1+\Delta)\phi^n\|^2 + \|(1+\Delta)(\phi^{n+1} - \phi^n)\|^2\Big).\end{aligned} \tag{3.29}$$

Thirdly, by taking the L^2 inner product of (3.7d) with $2U^{n+1}$, we obtain

$$\|U^{n+1}\|^2 - \|U^n\|^2 + \|U^{n+1} - U^n\|^2 = \left(H(\phi^n)\left(\phi^{n+1} - \phi^n\right), U^{n+1}\right). \tag{3.30}$$

Fourthly, define $p^{n+1} = \Delta^{-1}\psi^{n+1}$. By subtracting with the nth step, we obtain

$$\Delta(p^{n+1} - p^n) = \psi^{n+1} - \psi^n. \tag{3.31}$$

From (3.7c) and (3.31), we derive

$$\begin{aligned}\frac{1}{\delta t M}\left(\Delta^{-1}\left(\psi^{n+1}-\psi^{n}\right),\phi^{n+1}-\phi^{n}\right)&=\frac{1}{M}\left(p^{n+1}-p^{n},\psi^{n+1}\right)\\&=\frac{1}{M}\left(p^{n+1}-p^{n},\Delta p^{n+1}\right)\\&=-\frac{1}{2M}\left(\|\nabla p^{n+1}\|^{2}-\|\nabla p^{n}\|^{2}+\|\nabla(p^{n+1}-p^{n})\|^{2}\right),\end{aligned}\tag{3.32}$$

and

$$\begin{aligned}\frac{\beta}{M}\left(\Delta^{-1}\psi^{n+1},\phi^{n+1}-\phi^{n}\right)&=\frac{\delta t\beta}{M}(p^{n+1},\psi^{n+1})=\frac{\delta t\beta}{M}(p^{n+1},\Delta p^{n+1}))\\&=-\frac{\delta t\beta}{M}\|\nabla p^{n+1}\|^{2}.\end{aligned}\tag{3.33}$$

Finally, by combining (3.29), (3.30), (3.32), and (3.33), we obtain

$$\begin{aligned}\|U^{n+1}\|^{2}-\|U^{n}\|^{2}&+\frac{1}{2}\left(\|(1+\Delta)\phi^{n+1}\|^{2}-\|(1+\Delta)\phi^{n}\|^{2}\right)\\&+\frac{1}{2M}\left(\|\nabla p^{n+1}\|^{2}-\|\nabla p^{n}\|^{2}\right)\\&+\|U^{n+1}-U^{n}\|^{2}+\frac{1}{2}\|(1+\Delta)(\phi^{n+1}-\phi^{n})\|^{2}\\&+\frac{1}{2M}\|\nabla(p^{n+1}-p^{n})\|^{2}=-\frac{\delta t\beta}{M}\|\nabla p^{n+1}\|^{2},\end{aligned}\tag{3.34}$$

that concludes the result (3.25) after dropping some positive terms. □

3.2 The Crank–Nicolson scheme

A second-order scheme, based on the Crank–Nicolson method, reads as follows.

Scheme 2 Assuming that $(\phi^{n-1},\ \psi^{n-1},\ U^{n-1})$ and $(\phi^{n},\ \psi^{n},\ U^{n})$ are already calculated with $n\geq 1$, we then update $(\phi^{n+1},\ \psi^{n+1},\ U^{n+1})$ as follows,

$$\frac{\psi^{n+1}-\psi^{n}}{\delta t}+\beta\frac{\psi^{n+1}+\psi^{n}}{2}=M\Delta\mu^{n+\frac{1}{2}},\tag{3.35a}$$

$$\mu^{n+\frac{1}{2}}=H^{\dagger,n+1}\frac{U^{n+1}+U^{n}}{2}+(1+\Delta)^{2}\frac{\phi^{n+1}+\phi^{n}}{2},\tag{3.35b}$$

$$\frac{\psi^{n+1}+\psi^{n}}{2}=\frac{\phi^{n+1}-\phi^{n}}{\delta t},\tag{3.35c}$$

$$U^{n+1}-U^{n}=\frac{1}{2}H^{\dagger,n+1}(\phi^{n+1}-\phi^{n}),\tag{3.35d}$$

where

$$H^{\dagger,n+1}=\frac{f(\phi^{\dagger,n+1})}{\sqrt{F(\phi^{\dagger,n+1})+B}},\quad \phi^{\dagger,n+1}=\frac{3}{2}\phi^{n}-\frac{1}{2}\phi^{n-1}.\tag{3.36}$$

We can rewrite the equations (3.35c) and (3.35d) as follows,

$$\begin{cases} U^{n+1} = \dfrac{1}{2} H^{\dagger,n+1}\phi^{n+1} + h_1^n, & (3.37) \\ \psi^{n+1} = \dfrac{2}{\delta t}\phi^{n+1} + h_2^n, & (3.38) \end{cases}$$

where $h_1^n = (U^n - \frac{1}{2}H^{\dagger,n+1}\phi^n)$, $h_2^n = -\frac{2}{\delta t}\phi^n - \psi^n$. Thus, (3.35a) and (3.35b) can be rewritten as the following linear system

$$\alpha^{\dagger}\phi^{n+1} = M\Delta\mu^{n+1} + h_3^n, \tag{3.39}$$

$$\mu^{n+\frac{1}{2}} = P_2(\phi^{n+1}) + h_4^n, \tag{3.40}$$

where

$$\begin{cases} \alpha^{\dagger} = \left(\dfrac{1}{\delta t} + \dfrac{\beta}{2}\right)\dfrac{2}{\delta t}, \\ P_2(\phi^{n+1}) = \dfrac{1}{4}H^{\dagger,n+1}H^{\dagger,n+1}\phi^{n+1} + \dfrac{1}{2}(1+\Delta)^2\phi^{n+1}, \\ h_3^n = -\left(\dfrac{1}{\delta t} + \dfrac{\beta}{2}\right)h_2^n + \left(\dfrac{1}{\delta t} - \dfrac{\beta}{2}\right)\psi^n, \\ h_4^n = \dfrac{1}{2}H^{\dagger,n+1}h_1^n + \dfrac{1}{2}H^{\dagger}U^n + \dfrac{1}{2}(1+\Delta)^2\phi^{n+1}. \end{cases} \tag{3.41}$$

Actually, we can solve ϕ^{n+1} and μ^{n+1} directly from (3.39) and (3.40). Once we obtain ϕ^{n+1}, U^{n+1} and ψ^{n+1} are automatically given in (3.37)–(3.38). Furthermore, we notice

$$\big(P_2(\phi), \psi\big) = \frac{1}{4}\big(H^{\dagger,n+1}\phi, H^{\dagger,n+1}\psi\big) + \frac{1}{2}\big((1+\Delta)\phi, (1+\Delta)\psi\big), \tag{3.42}$$

if ψ enjoys the same boundary condition as ϕ. Therefore, the linear operator $P_2(\cdot)$ is symmetric (self-adjoint). Moreover, for any ϕ with $\int_\Omega \phi\, dx = 0$, we have

$$\big(P_2(\phi), \phi\big) = \frac{1}{4}\|H^{\dagger,n+1}\phi\|^2 + \frac{1}{2}\|(1+\Delta)\phi\|^2 \geq 0, \tag{3.43}$$

where "= " is valid if and only if $\phi \equiv 0$.

Theorem 3 *The scheme* (3.35a)–(3.35d) *(or* (3.39)–(3.40)*) is unconditionally energy stable satisfying the following discrete energy dissipation law*

$$E_{cn2}^{n+1} - E_{cn2}^{n} = -\frac{\delta t\beta}{M}\left\|\frac{\nabla(p^{n+1}+p^n)}{2}\right\|^2 \leq 0, \tag{3.44}$$

where

$$E_{cn2} = \|U\|^2 + \frac{1}{2}\|(1+\Delta)\phi\|^2 + \frac{1}{2M}\|\nabla p\|^2 - B|\Omega|. \tag{3.45}$$

Proof Firstly, we combine (3.35a) and (3.35b) together and apply the Δ^{-1} to obtain

$$\frac{1}{\delta t M}\Delta^{-1}\left(\psi^{n+1}-\psi^{n}\right)+\frac{\beta}{2M}\Delta^{-1}\left(\psi^{n+1}+\psi^{n}\right)=H^{\dagger,n+1}\frac{U^{n+1}+U^{n}}{2}+(1+\Delta)^{2}\frac{\phi^{n+1}+\phi^{n}}{2}. \tag{3.46}$$

Secondly, by taking the L^2 inner product of (3.46) with $\phi^{n+1}-\phi^{n}$, we obtain

$$\begin{aligned}&\frac{1}{\delta t M}\left(\Delta^{-1}\left(\psi^{n+1}-\psi^{n}\right),\phi^{n+1}-\phi^{n}\right)+\frac{\beta}{2M}\left(\Delta^{-1}\left(\psi^{n+1}+\psi^{n}\right),\phi^{n+1}-\phi^{n}\right)\\&\quad=\left(H\dagger\frac{U^{n+1}+U^{n}}{2},\phi^{n+1}-\phi^{n}\right)+\frac{1}{2}\left(\|(1+\Delta)\phi^{n+1}\|^{2}-\|(1+\Delta)\phi^{n}\|^{2}\right).\end{aligned} \tag{3.47}$$

Thirdly, by taking the L^2 inner product of (3.35d) with $U^{n+1}+U^{n}$, we obtain

$$\|U^{n+1}\|^{2}-\|U^{n}\|^{2}=\left(\frac{1}{2}H^{\dagger,n+1}\left(\phi^{n+1}-\phi^{n}\right),U^{n+1}+U^{n}\right). \tag{3.48}$$

From (3.35c) and (3.31), we derive

$$\begin{aligned}&\frac{1}{\delta t M}\left(\Delta^{-1}\left(\psi^{n+1}-\psi^{n}\right),\phi^{n+1}-\phi^{n}\right)=\frac{1}{2M}\left(p^{n+1}-p^{n},\psi^{n+1}+\psi^{n}\right)\\&\quad=\frac{1}{2M}\left(p^{n+1}-p^{n},\Delta(p^{n+1}+p^{n})\right)=-\frac{1}{2M}\left(\|\nabla p^{n+1}\|^{2}-\|\nabla p^{n}\|^{2}\right),\end{aligned} \tag{3.49}$$

and

$$\begin{aligned}&\frac{\beta}{2M}\left(\Delta^{-1}\left(\psi^{n+1}+\psi^{n}\right),\phi^{n+1}-\phi^{n}\right)=\frac{\delta t\beta}{4M}\left(p^{n+1}+p^{n},\psi^{n+1}+\psi^{n}\right)\\&\quad=\frac{\delta t\beta}{4M}\left(p^{n+1}+p^{n},\Delta(p^{n+1}+p^{n})\right)=-\frac{\delta t\beta}{M}\left\|\frac{\nabla(p^{n+1}+p^{n})}{2}\right\|^{2}.\end{aligned} \tag{3.50}$$

Finally, by combining (3.47), (3.48), (3.49), and (3.50), we obtain

$$\begin{aligned}&\|U^{n+1}\|^{2}-\|U^{n}\|^{2}+\frac{1}{2}\left(\|(1+\Delta)\phi^{n+1}\|^{2}-\|(1+\Delta)\phi^{n}\|^{2}\right)\\&\quad+\frac{1}{2M}\left(\|\nabla p^{n+1}\|^{2}-\|\nabla p^{n}\|^{2}\right)=-\frac{\delta t\beta}{M}\left\|\frac{\nabla(p^{n+1}+p^{n})}{2}\right\|^{2},\end{aligned} \tag{3.51}$$

that implies the desired result (3.44). □

3.3 The BDF2 scheme

We also can easily develop an alternative version of second-order scheme based on the Adams–Bashforth backward differentiation formulas (BDF2).

Scheme 3 Assuming that $(\phi^{n-1},\ \psi^{n-1},\ U^{n-1})$ and $(\phi^{n},\ \psi^{n},\ U^{n})$ are already calculated with $n \geq 1$, we then update $(\phi^{n+1},\ \psi^{n+1},\ U^{n+1})$ as follows:

$$\frac{3\psi^{n+1}-4\psi^{n}+\psi^{n-1}}{2\delta t}+\beta\psi^{n+1}=M\Delta\mu^{n+1}, \tag{3.52a}$$

$$\mu^{n+1}=H^{\star,n+1}U^{n+1}+(1+\Delta)^2\phi^{n+1}, \tag{3.52b}$$

$$\psi^{n+1}=\frac{3\phi^{n+1}-4\phi^{n}+\phi^{n-1}}{2\delta t}, \tag{3.52c}$$

$$3U^{n+1}-4U^{n}+U^{n-1}=\frac{1}{2}H^{\star,n+1}\left(3\phi^{n+1}-4\phi^{n}+\phi^{n-1}\right), \tag{3.52d}$$

where

$$H^{\star,n+1}=\frac{f(\phi^{\star,n+1})}{\sqrt{F(\phi^{\star,n+1})+B}},\quad \phi^{\star,n+1}=2\phi^{n}-\phi^{n-1}. \tag{3.53}$$

We can rewrite the equations (3.52c) and (3.52d) as follows:

$$\begin{cases} U^{n+1}=\dfrac{1}{2}H^{\star,n+1}\phi^{n+1}+q_1^{n}, & (3.54)\\ \psi^{n+1}=\dfrac{3}{2\delta t}\phi^{n+1}+q_2^{n}, & (3.55) \end{cases}$$

where $q_1^n=U^{\pm}-\frac{1}{2}H^{\star,n+1}\phi^{\pm}$, $q_2^n=-\frac{3}{2\delta t}\phi^{\pm}$ with $S^{\pm}=\frac{4S^n-S^{n-1}}{3}$ for any variable S. Thus, (3.52a) and (3.54)–(3.55) can be rewritten as the following linear system

$$\alpha^{\star}\phi^{n+1}=M\Delta\mu^{n+1}+q_3^{n}, \tag{3.56}$$

$$\mu^{n+1}=P_3(\phi^{n+1})+q_4^{n}, \tag{3.57}$$

where

$$\begin{cases} \alpha^{\star}=\left(\dfrac{3}{2\delta t}+\beta\right)\dfrac{3}{2\delta t},\\ P_3(\phi^{n+1})=\dfrac{1}{2}H^{\star,n+1}H^{\star,n+1}\phi^{n+1}+(1+\Delta)^2\phi^{n+1},\\ q_3^{n}=-\left(\dfrac{3}{2\delta t}+\beta\right)q_2^{n}+\dfrac{3}{2\delta t}\psi^{\pm},\\ q_4^{n}=H^{\star,n+1}q_1^{n}. \end{cases} \tag{3.58}$$

Therefore, we can solve ϕ^{n+1} and μ^{n+1} directly from (3.56) and (3.57). Once we obtain ϕ^{n+1}, U^{n+1} and ψ^{n+1} are automatically given in (3.58). Furthermore, we notice

$$\big(P_3(\phi),\psi\big)=\frac{1}{2}\big(H^{\star,n+1}\phi,H^{\star,n+1}\psi\big)+\big((1+\Delta)\phi,(1+\Delta)\psi\big), \tag{3.59}$$

if ψ enjoys the same boundary condition as ϕ. Therefore, the linear operator $P_3(\cdot)$ is symmetric (self-adjoint). Moreover, for any ϕ with $\int_\Omega \phi\,dx=0$, we have

$$\big(P_3(\phi),\phi\big)=\frac{1}{2}\|H^{\star,n+1}\phi\|^2+\|(1+\Delta)\phi\|^2\geq 0, \tag{3.60}$$

where "= " is valid if and only if $\phi\equiv 0$.

Theorem 4 *The scheme (3.52a)–(3.52d) (or (3.56)–(3.57)) is unconditionally energy stable satisfying the following discrete energy dissipation law*

$$E_{bdf2}^{n+1,n} - E_{bdf2}^{n,n-1} \leq -\frac{\delta t\beta}{M}\|\nabla p^{n+1}\|^2 \leq 0, \tag{3.61}$$

where

$$\begin{aligned} E_{bdf2}^{n+1,n} =& \frac{\|U^{n+1}\|^2 + \|2U^{n+1} - U^n\|^2}{2} \\ &+ \frac{1}{2}\left(\frac{\|(1+\Delta)\phi^{n+1}\|^2 + \|(1+\Delta)(2\phi^{n+1} - \phi^n)\|^2}{2}\right) \\ &+ \frac{1}{2M}\left(\frac{\|\nabla p^{n+1}\|^2 + \|2\nabla p^{n+1} - \nabla p^n\|^2}{2}\right) - B|\Omega|. \end{aligned} \tag{3.62}$$

Proof Firstly, we combine (3.52a) and (3.52b) together and apply the Δ^{-1} to obtain

$$\frac{1}{2\delta t M}\Delta^{-1}\left(3\psi^{n+1} - 4\psi^n + \psi^{n-1}\right) + \frac{\beta}{M}\Delta^{-1}\psi^{n+1} = H^{\star,n+1}U^{n+1} + (1+\Delta)^2\phi^{n+1}. \tag{3.63}$$

Secondly, by taking the L^2 inner product of (3.63) with $3\phi^{n+1} - 4\phi^n + \phi^{n-1}$, and applying the following identity

$$(3a - 4b + c, 2a) = a^2 - b^2 + (2a - b)^2 - (2b - c)^2 + (a - 2b + c)^2, \tag{3.64}$$

we obtain

$$\begin{aligned} &\frac{1}{2\delta t M}\left(\Delta^{-1}\left(3\psi^{n+1} - 4\psi^n + \psi^{n-1}\right), 3\phi^{n+1} - 4\phi^n + \phi^{n-1}\right) \\ &\quad + \frac{\beta}{M}\left(\Delta^{-1}\psi^{n+1}, 3\phi^{n+1} - 4\phi^n + \phi^{n-1}\right) \\ &= \left(H^{\star,n+1}U^{n+1}, 3\phi^{n+1} - 4\phi^n + \phi^{n-1}\right) \\ &\quad + \frac{1}{2}\Big(\|(1+\Delta)\phi^{n+1}\|^2 - \|(1+\Delta)\phi^n\|^2 + \|(1+\Delta)(2\phi^{n+1} - \phi^n)\|^2 \\ &\quad - \|(1+\Delta)(2\phi^n - \phi^{n-1})\|^2 + \|(1+\Delta)(\phi^{n+1} - 2\phi^n + \phi^{n-1})\|^2\Big). \end{aligned} \tag{3.65}$$

Thirdly, by taking the L^2 inner product of (3.52d) with $2U^{n+1}$, we obtain

$$\begin{aligned} &\|U^{n+1}\|^2 - \|U^n\|^2 + \|2U^{n+1} - U^n\|^2 - \|2U^n - U^{n-1}\|^2 \\ &\quad + \|U^{n+1} - 2U^n + U^{n-1}\|^2 \\ &\quad = \left(H^{\star,n+1}\left(3\phi^{n+1} - 4\phi^n + \phi^{n-1}\right), U^{n+1}\right). \end{aligned} \tag{3.66}$$

Fourthly, define $p^{n+1} = \Delta^{-1}\psi^{n+1}$. By subtracting with the nth and $(n-1)$th step, we obtain

$$\Delta(3p^{n+1} - 4p^n + p^{n-1}) = 3\psi^{n+1} - 4\psi^n + \psi^{n-1}. \tag{3.67}$$

From (3.52c) and (3.67), we derive

$$\begin{aligned}
&\frac{1}{2\delta t M}\left(\Delta^{-1}\left(3\psi^{n+1}-4\psi^{n}+\psi^{n-1}\right),3\phi^{n+1}-4\phi^{n}+\psi^{n-1}\right)\\
&\quad=\frac{1}{M}\left(3p^{n+1}-4p^{n}+p^{n-1},\psi^{n+1}\right)=\frac{1}{M}\left(3p^{n+1}-4p^{n}+p^{n-1},\Delta p^{n+1}\right)\\
&\quad=-\frac{1}{2M}\Big(\|\nabla p^{n+1}\|^2-\|\nabla p^{n}\|^2+\|2\nabla p^{n+1}-\nabla p^{n}\|^2-\|2\nabla p^{n}-\nabla p^{n-1}\|^2\\
&\qquad\qquad+\|\nabla(p^{n+1}-2p^{n}-p^{n-1})\|^2\Big),
\end{aligned}\tag{3.68}$$

and

$$\begin{aligned}
&\frac{\beta}{M}\left(\Delta^{-1}\psi^{n+1},3\phi^{n+1}-4\phi^{n}+\phi^{n-1}\right)\\
&\quad=\frac{2\delta t\beta}{M}\left(p^{n+1},\psi^{n+1}\right)=\frac{2\delta t\beta}{M}\left(p^{n+1},\Delta p^{n+1}\right)=-\frac{2\delta t\beta}{M}\|\nabla p^{n+1}\|^2.
\end{aligned}\tag{3.69}$$

Finally, by combining (3.65), (3.66), (3.68), and (3.69), we obtain

$$\begin{aligned}
&\|U^{n+1}\|^2-\|U^{n}\|^2+\|2U^{n+1}-U^{n}\|^2-\|2U^{n}-U^{n-1}\|^2\\
&+\frac{1}{2}\Big(\|(1+\Delta)\phi^{n+1}\|^2-\|(1+\Delta)\phi^{n}\|^2+\|(1+\Delta)(2\phi^{n+1}-\phi^{n})\|^2\\
&-\|(1+\Delta)(2\phi^{n}-\phi^{n-1})\|^2\Big)\\
&+\frac{1}{2M}\Big(\|\nabla p^{n+1}\|^2-\|\nabla p^{n}\|^2+\|\nabla(2p^{n+1}-p^{n})\|^2-\|\nabla(2p^{n}-p^{n-1})\|^2\Big)\\
&+\|U^{n+1}-2U^{n}+U^{n-1}\|^2+\frac{1}{2}\|(1+\Delta)(\phi^{n+1}-2\phi^{n}+\phi^{n-1})\|^2\\
&+\frac{1}{2M}\|\nabla(p^{n+1}-2p^{n}-p^{n-1})\|^2\\
&=-\frac{2\delta t\beta}{M}\|\nabla p^{n+1}\|^2,
\end{aligned}\tag{3.70}$$

which implies the result (3.61) after dropping some positive terms. □

Remark 4 Note that the energy E_{cn2} in (3.45) coincides with E_{1st} in (3.26). In addition, we emphasize the discrete energy of the Crank–Nicolson scheme strictly follows the PDE energy law (3.6) (i.e., "=" instead of "≤").

Remark 5 Similar to the first-order scheme (3.7) (or (3.11)–(3.12)), we can show the linear system (3.35) (or (3.39)–(3.40)) and (3.52) (or (3.56)–(3.57)) are symmetric and positive definite; thus, their well-posedness is available as well. The proof follows in a similar manner as that of Theorem 1. We omit the details for brevity.

Remark 6 The linear systems (3.7), (3.35), and (3.52) are symmetric and positive definite; thus, a fast solver such as the preconditioned conjugate gradient (PCG) method can be used to solve the systems.

Remark 7 Both of the second-order schemes (3.35) and (3.52) couple three time levels and $(\phi^{n+1}, \psi^{n+1}, U^{n+1})$ can be updated repeatedly by the recurrence relation once the initial values (ϕ^0, ψ^0, U^0) and (ϕ^1, ψ^1, U^1) have been computed. Here, (ϕ^0, ψ^0, U^0) is determined by the initial conditions. In order to obtain the second-order time accuracy of the main scheme, we first compute $(\tilde{\phi}^1, \tilde{\psi}^1, \tilde{U}^1)$ by the first-order scheme (3.7), then use the following corrector scheme to obtain (ϕ^1, ψ^1, U^1),

$$\frac{\psi^1 - \psi^0}{\delta t} + \beta \frac{\psi^1 + \psi^0}{2} = M \Delta \mu^{\frac{1}{2}}, \tag{3.71a}$$

$$\mu^{\frac{1}{2}} = H^{\ddagger,1} \frac{U^1 + U^0}{2} + (1 + \Delta)^2 \frac{\phi^1 + \phi^0}{2}, \tag{3.71b}$$

$$\frac{\psi^1 + \psi^0}{2} = \frac{\phi^1 - \phi^0}{\delta t}, \tag{3.71c}$$

$$U^1 - U^0 = \frac{1}{2} H^{\ddagger,1} (\phi^1 - \phi^0), \tag{3.71d}$$

where

$$H^{\ddagger,1} = \frac{f(\phi^{\ddagger,1})}{\sqrt{F(\phi^{\ddagger,1}) + B}}, \quad \phi^{\ddagger,1} = \tilde{\phi}^1. \tag{3.72}$$

4 Fourier spectral fully discrete scheme and implementation

Generally, our time-marching schemes can carry over to any spatial discretization (e.g., finite difference [1, 25], finite element [11, 15], radial basis function [7] methods) as long as the spatial discretization provides the desired tolerance. In this paper, we assume the periodic boundary condition and focus on time discretization. Therefore, we use the Fourier spectral method for the spatial discretization and the fast Fourier transform (FFT) is applied for all numerical simulations to solve the MPFC equation with the periodic boundary condition.

For brevity, we only consider the two-dimensional fully discrete Crank–Nicolson schemes in this section. Other fully discrete schemes in one-dimensional or three-dimensional cases are constructed analogously. Let N_x and N_y be two positive even integers. The spatial domain $\Omega = [a_1, b_1] \times [a_2, b_2]$ is uniformly partitioned with mesh size $h_x = (b_1 - a_1)/N_x$, $h_y = (b_2 - a_2)/N_y$ and

$$\Omega_h = \left\{ (x_i, y_j) \middle| x_i = a_1 + i h_x,\ y_j = a_2 + j h_y,\ 0 \le i \le N_x - 1,\ 0 \le j \le N_y - 1 \right\}. \tag{4.1}$$

Let $V_h = \left\{ u \middle| u = \{u_{ij} | (x_i, y_j) \in \Omega_h\} \right\}$ be the space of grid functions on Ω_h. The time semi-discrete solution $u^n(x, y)$ can be approximated by

$$u^n(x, y) \approx u_N^n(x, y) := \sum_{k=-N_x/2}^{N_x/2-1} \sum_{l=-N_y/2}^{N_y/2-1} \hat{u}_{kl}^n e^{\mathrm{i}\xi_k x + \mathrm{i}\eta_l y}, \tag{4.2}$$

where $\mathrm{i} = \sqrt{-1}$, $\hat{u}_{kl}^n$ are the Fourier coefficient of u^n, $\xi_k = 2\pi k/(b_1 - a_1)$, $\eta_l = 2\pi l/(b_2 - a_2)$, $k = -N_x/2, \ldots, N_x/2 - 1$, and $l = -N_y/2, \ldots, N_y/2 - 1$. Then, based on the scheme (3.35), the fully discrete Crank–Nicolson scheme reads:

Assuming that $(\phi_N^{n-1}, \psi_N^{n-1}, U_N^{n-1})$ and $(\phi_N^n, \psi_N^n, U_N^n)$ are already calculated with $n \geq 1$, we then update $(\phi_N^{n+1}, \psi_N^{n+1}, U_N^{n+1})$ as follows:

$$\frac{\psi_N^{n+1} - \psi_N^n}{\delta t} + \beta \frac{\psi_N^{n+1} + \psi_N^n}{2} = M\Delta_N \mu_N^{n+\frac{1}{2}}, \tag{4.3a}$$

$$\mu_N^{n+\frac{1}{2}} = H_N^{\dagger,n+1} \frac{U_N^{n+1} + U_N^n}{2} + (1+\Delta_N)^2 \frac{\phi_N^{n+1} + \phi_N^n}{2}, \tag{4.3b}$$

$$\frac{\psi_N^{n+1} + \psi_N^n}{2} = \frac{\phi_N^{n+1} - \phi_N^n}{\delta t}, \tag{4.3c}$$

$$U_N^{n+1} - U_N^n = \frac{1}{2} H_N^{\dagger,n+1} (\phi_N^{n+1} - \phi_N^n), \tag{4.3d}$$

where

$$H_N^{\dagger,n+1} = \frac{f(\phi_N^{\dagger,n+1})}{\sqrt{F(\phi_N^{\dagger,n+1}) + B}}, \quad \phi_N^{\dagger,n+1} = \frac{3}{2}\phi_N^n - \frac{1}{2}\phi_N^{n-1}. \tag{4.4}$$

Here, the discrete Laplace operator Δ_N is defined as

$$\Delta_N := \mathcal{F}_N^{-1}(-\Lambda)\mathcal{F}_N, \tag{4.5}$$

where $(\Lambda)_{k,l} = \xi_k^2 + \eta_l^2$, $(k = -N_x/2, \ldots, N_x/2 - 1,\ l = -N_y/2, \ldots, N_y/2 - 1)$, $\mathcal{F}_N$ is the discrete Fourier transform, and $\mathcal{F}_N^{-1}$ is the discrete inverse Fourier transform.

Using (3.37)–(3.41), we obtain

$$\alpha^\dagger \phi_N^{n+1} - M\Delta_N \left(P_2(\phi_N^{n+1}) \right) = RHS, \tag{4.6}$$

where RHS is approximation of $M\Delta h_4^n + h_3^n$.

In this paper, the preconditioned conjugate gradient (PCG) method is used to solve the system (4.6) and we use the following preconditioner $P^\dagger$ to accelerate the convergence speed of the PCG algorithm,

$$P^\dagger = \alpha^\dagger I - M\Delta_N \left(\frac{1}{4}\overline{H^{\dagger,n+1} H^{\dagger,n+1}} + \frac{1}{2}(1+\Delta_N)^2 \right), \tag{4.7}$$

where I is the identity matrix, and $\overline{(\cdot)}$ is the average value of $(\cdot)$.

Remark 8 For the first-order scheme and the BDF2 scheme, we use the following preconditioners P^* and $P^\star$, respectively,

$$\begin{aligned} P^* &= \alpha^* I - M\Delta_N \left(\frac{1}{2}\overline{H(\phi_N^n) H(\phi_N^n)} + (1+\Delta_N)^2 \right), \\ P^\star &= \alpha^\star I - M\Delta_N \left(\frac{1}{2}\overline{H^{\star,n+1} H^{\star,n+1}} + (1+\Delta_N)^2 \right). \end{aligned} \tag{4.8}$$

5 Numerical experiments

We now present various 2D and 3D numerical simulations for the MPFC equation to demonstrate the accuracy, stability, and efficiency of the proposed schemes. The stopping criterion for the PCG iteration is that a relative residual is less than a $tol = 10^{-12}$ unless mentioned otherwise.

5.1 Temporal accuracy test

We test the convergence rates of the three proposed schemes, the first-order scheme (3.7) (denoted by LS1), the second-order Crank–Nicolson scheme (3.35) (denoted by CN2), and the second-order BDF2 scheme (3.52) (denoted by BDF2). The parameters are $\epsilon = 0.025$, $\beta = 0.9$, $M = 1$.

We perform two numerical simulations to test the accuracy. In the first example, we choose the suitable forcing term such that the exact solution is given by

$$\phi(x, y, t) = \sin(\frac{2\pi}{64}x)\cos(\frac{2\pi}{64}x)\cos(t). \tag{5.1}$$

The computational domain is set to be $\Omega = [0, 128]^2$. We use 256^2 Fourier modes so that the errors from the spatial discretization are negligible compared with the time discretization errors. In Table 1, we list the L^2 errors of the phase variable between the numerical solution and the exact solution at $T = 20$ with different time step sizes.

In the second example, we perform the mesh refinement test of the time step size with the following initial condition

$$\begin{aligned}\phi^0(x, y) \;=\; & 0.07 - 0.02\cos\left(\frac{2\pi(x-12)}{32}\right)\sin\left(\frac{2\pi(y-1)}{32}\right) \\ & + 0.02\cos^2\left(\frac{\pi(x+10)}{32}\right)\cos^2\left(\frac{\pi(y+3)}{32}\right) \\ & - 0.01\sin^2\left(\frac{4\pi x}{32}\right)\sin^2\left(\frac{4\pi(y-6)}{32}\right).\end{aligned} \tag{5.2}$$

Table 1 The L^2 errors at $T = 20$ for the phase variable ϕ that are computed by LS1, CN2, and BDF2 schemes using different temporal resolutions

δt	LS1	Order	CN2	Order	BDF2	Order
0.2000	2.5442e−01	–	3.9077e−03	–	4.8011e−03	–
0.1000	1.4257e−01	0.84	9.3243e−04	2.07	2.3359e−03	1.04
0.0500	7.5271e−02	0.92	2.3055e−04	2.02	7.4908e−04	1.64
0.0200	3.1074e−02	0.97	3.6812e−05	2.00	1.3622e−04	1.86
0.0100	1.5698e−02	0.99	9.2042e−06	2.00	3.5430e−05	1.94
0.0050	7.8896e−03	0.99	2.3019e−06	2.00	9.0297e−06	1.97

The exact solution is given in (5.1) with parameters $\epsilon = 0.025$, $\beta = 0.9$, and $M = 1$ and 256^2 Fourier modes for space

The computational domain is set to be $\Omega = [0, 32]^2$. We use 128^2 Fourier modes and choose the approximate solution obtained by using CN2 with a small time step size $\delta t = 0.001$ as the benchmark solution (approximately the exact solution) for computing errors. In Table 2, we list the L^2 errors of the phase variable between the numerical solution and the benchmark solution at $T = 20$ with different time step sizes.

From Tables 1 and 2, we can observe that all schemes give desired orders of accuracy in time. LS1 is first-order accurate in time, while CN2 and BDF2 are second-order accurate in time. CN2 and BDF2 give much better accuracy than LS1. CN2 performs slightly better than BDF2 when using the same time step.

5.2 Comparison with convex splitting schemes

Below, we make a comparison between our schemes proposed in this paper with two kinds of convex splitting schemes proposed in [1] and [17]. The first- and second-order convex splitting schemes in [1] are denoted by $\mathrm{CS}_{DF}1$ and $\mathrm{CS}_{DF}2$, respectively. And the new first- and second-order convex splitting schemes in [17] are denoted by $\mathrm{CS}_{BF}1$ and $\mathrm{CS}_{BF}2$, respectively. Both kinds of convex splitting schemes are nonlinear, and need to be solved by Newton's iteration at each time step. Here, the biconjugate gradients (BICG) method is used to solve linear systems due to the absence of symmetric positive definite properties. The stopping criterion for the BICG iteration is that the relative residual norm is less than $tol = 10^{-8}\delta t$. Readers can refer to [1] and [17] for more details on the implementation of these schemes.

Firstly, we choose the initial data (5.2) to compare the accuracy of the numerical schemes. Figure 1 shows the L^2 errors using the mesh refinement at $T = 20$ and $T = 50$ with different time step sizes. It is observed that all schemes of $\mathrm{CS}_{DF}1$, $\mathrm{CS}_{DF}2$, $\mathrm{CS}_{BF}1$, $\mathrm{CS}_{BF}2$, LS1, CN2, and BDF2 give the desired order of accuracy in time. It is noteworthy that the error curves of $\mathrm{CS}_{BF}1$ and LS1, and $\mathrm{CS}_{BF}2$ and CN2 almost overlap, and the accuracy of CS_{BF} and our schemes are better than that of CS_{DF} when using the same time step.

Table 2 The L^2 errors at $T = 20$ for the phase variable ϕ that are computed by LS1, CN2, and BDF2 schemes using different temporal resolutions

δt	LS1	Order	CN2	Order	BDF2	Order
4.0000	3.6931e−03	–	2.5094e−04	–	9.0028e−04	–
2.0000	1.9249e−03	0.94	6.3159e−05	1.99	2.2297e−04	2.01
1.0000	9.8280e−04	0.97	1.5181e−05	2.06	5.4456e−05	2.03
0.5000	4.9660e−04	0.98	3.6378e−06	2.06	1.3341e−05	2.03
0.2500	2.4961e−04	0.99	8.7965e−07	2.05	3.2867e−06	2.02
0.1250	1.2514e−04	1.00	2.1579e−07	2.03	8.1372e−07	2.01

Using the approximate solution obtained by the scheme CN2 with a small time step size $\delta t = 0.001$ as the benchmark solution to calculate the L^2 errors with parameters $\epsilon = 0.025$, $\beta = 0.9$, and $M = 1$ and 128^2 Fourier modes for space

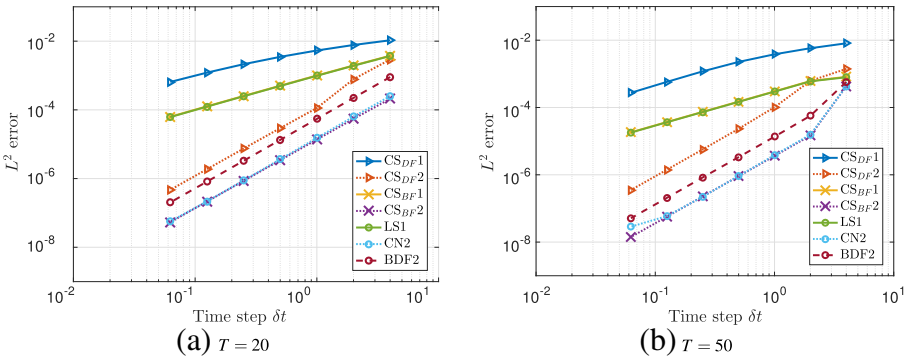

Fig. 1 The L^2 errors at $T = 20$ and $T = 50$ for the phase variable ϕ with different temporal resolutions. Using the approximate solution obtained by the time step size $\delta t = 0.001$ as the benchmark solution to calculate the L^2 Fourier modes for space

Secondly, Table 3 lists the average number of iterations (N-iter) and the average number of solving linear system (N-sol) at each time step and CPU time (in seconds) of schemes CS$_{DF}$1, CS$_{DF}$2, CS$_{BF}$1, CS$_{BF}$2, LS1, CN2, and BDF2 with different time step sizes. It can be observed clearly that the convex splitting schemes CS$_{DF}$ and CS$_{BF}$ require more CPU time than linear schemes LS1, CN2, and BDF2. The reason is that the nonlinear schemes CS$_{DF}$ and CS$_{BF}$ require Newton's iteration method to solve nonlinear systems at each time step. So these schemes need to solve more linear systems and therefore require more CPU time. In addition, the linear systems corresponding to linear schemes LS1, CN2, and BDF2 are symmetric positive definite; therefore, the PCG method is very efficient and requires less CPU time. Among the three linear schemes, BDF2 requires the least CPU time.

5.3 Energy stability test

In this subsection, we choose the smooth initial data (5.2) to demonstrate the energy stability of proposed schemes. The parameters are $\epsilon = 0.025$, $M = 1$, $T = 100$, and $\Omega = [0, 32]^2$. We use 128^2 Fourier modes for spatial discretization.

In Fig. 2, we plot the evolution of energy E defined in (2.1), pseudo energy $\mathcal{E}$ defined in (2.12), and modified discrete energies E_{1st} defined in (3.26), E_{cn2} defined in (3.45), and E_{bdf2} defined in (3.62), which are calculated by LS1, CN2, and BDF2, respectively, where $\beta = 0.01$ and $\delta t = 0.01$. The pseudo energy $\mathcal{E}$ and modified discrete energies E_{1st}, E_{cn2}, and E_{bdf2} are non-increasing in time, while energy E may increase in time on some time intervals. In addition, the pseudo energy $\mathcal{E}$ are nearly identical to the modified energies E_{1st}, E_{cn2}, and E_{bdf2}. The above numerical results are consistent with Fig. 2 in [1] and Fig. 5 in [16].

In Fig. 3, we plot the evolution of the discrete energies E_{1st}, E_{cn2}, and E_{bdf2} with different time step sizes of $\delta t = 0.01$, 0.1, 1, 2,5, 10, 20, 25 using the schemes LS1, CN2, and BDF2, respectively, where $\beta = 2$. We observe that all the energies decay in time, which confirms that the proposed schemes are unconditionally energy stable, as predicted by Theorems 2, 3, and 4. Since schemes LS1, CN2, and BDF2 provide

Table 3 The average number of iterations (N-iter) and the average number of solving linear system (N-sol) at each time step and CPU time (in seconds) with parameters $T = 20$, $\epsilon = 0.025$, $\beta = 0.9$, and $M = 1$ and 128^2 Fourier modes for space

δt	N-iter	N-sol	CPU(s)	N-iter	N-sol	CPU(s)	N-iter	N-sol	CPU(s)	N-iter	N-sol	CPU(s)
	$CS_{DF}1$			$CS_{DF}2$			$CS_{BF}1$			$CS_{BF}2$		
4.0000	105.40	146.20	37.77	3.00	4.00	1.48	3.00	6.80	1.78	3.00	4.33	1.34
2.0000	51.30	69.90	36.47	3.00	3.40	1.59	3.00	5.80	3.00	3.00	4.00	1.92
1.0000	23.65	31.00	32.88	2.90	2.90	3.22	3.00	4.00	4.55	3.00	3.00	3.19
0.5000	11.88	14.35	31.89	2.35	2.35	5.06	2.75	3.75	8.66	2.40	2.40	5.03
0.2500	7.08	7.74	35.31	2.00	2.00	8.41	2.00	2.00	10.16	2.00	2.00	8.16
0.1250	5.00	5.00	49.20	2.00	2.00	16.66	2.00	2.00	20.13	2.00	2.00	16.33
	LS1			CN2			BDF2					
4.0000	1.00	3.00	0.36	1.00	2.40	0.50	1.00	2.67	0.48			
2.0000	1.00	2.80	0.80	1.00	2.20	0.70	1.00	2.60	0.45			
1.0000	1.00	2.25	1.30	1.00	2.00	1.31	1.00	2.00	0.69			
0.5000	1.00	2.00	2.05	1.00	2.00	2.33	1.00	2.00	1.11			
0.2500	1.00	2.00	4.17	1.00	2.00	4.72	1.00	2.00	2.14			
0.1250	1.00	2.00	8.09	1.00	1.69	8.56	1.00	2.00	4.28			

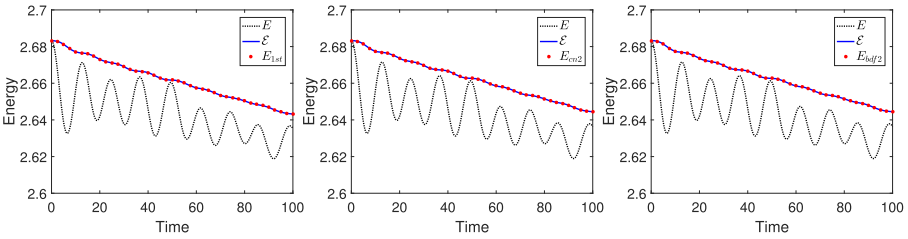

Fig. 2 Evolution of energy E defined in (2.1), pseudo energy $\mathcal{E}$ defined in (2.12), and modified discrete energies E_{1st} defined in (3.26), E_{cn2} defined in (3.45), and E_{bdf2} defined in (3.62) with parameters $\beta = 0.01$ and $\delta t = 0.01$

similar numerical results, without loss of generality, we only use scheme CN2 in the following discussion.

Figure 4 shows the evolution of the energy E, pseudo energy $\mathcal{E}$, and discrete energy E_{cn2} with $\beta = 10$, $\beta = 1$, and $\beta = 0.05$, respectively, where $\delta t = 0.01$. When β is large ($\beta = 10$, high damping case), the MPFC model behaves like the PFC model and $\mathcal{E}$ is nearly identical to E. On the other hand, when β is small ($\beta = 0.05$, low damping case), $\mathcal{E}$ differs from E and, in particular, E shows an oscillatory behavior unlike the case with $\beta = 10$. The above numerical results are consistent with the results in [17].

5.4 Phase transition behaviors in 2D and 3D

In this subsection, we use an alternative version of MPFC equation in the form of (2.13). With the computational domain of $[0, 32]^2$, and the initial data $\phi^0 = \bar{\phi}+$rand, where rand is uniformly distributed random number between -0.01 and 0.01 at the grid points, we use 128^2 Fourier modes to discretize the 2D space. The time step is $\delta t = 0.005$. The parameters are $\epsilon = 0.2$, $M = 1$, $\tilde{\beta} = 0.1$, and $T = 1000$. The scheme CN2 is used to examine the evolution from a random non-equilibrium state to a steady state.

Figure 5 presents the evolution of the phase transition behavior with $\bar{\phi} = 0.01$, $\bar{\phi} = 0.2$, and $\bar{\phi} = 0.4$, which verify that the proposed scheme CN2 does lead to the

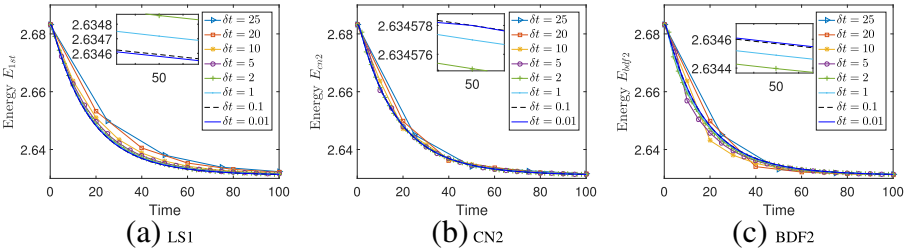

Fig. 3 Evolution of the energy with different time step size of $\delta t = 0.01$, 0.1, 1, 2,5, 10, 20, 25 using the schemes LS1, CN2, and BDF2, respectively, where $\beta = 2$

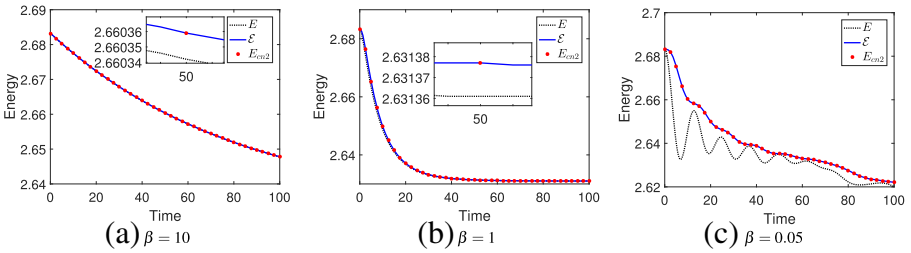

Fig. 4 Evolution of the energy E, pseudo energy $\mathcal{E}$ and discrete energy E_{cn2} with $\beta = 10$, 1 and 0.05 using the scheme CN2, where $\delta t = 0.01$

expected states in the phase diagram in [11]. With different values of $\bar{\phi}$, we obtain different patterns, such as stripes (Fig. 5a), stripes+triangles (Fig. 5b), and triangles (Fig. 5c). All of the numerical results are consistent with the phase diagram in [11]. In addition, Fig. 6 shows the evolution of the energy E_{cn2} for phase transition with

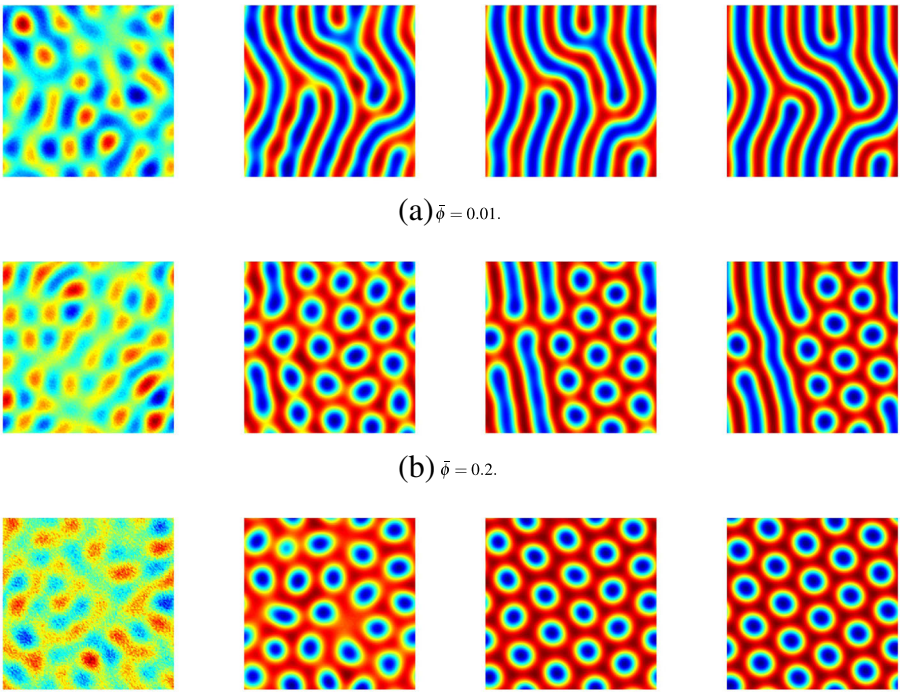

Fig. 5 The evolution of the phase transition behavior in 2D with $\bar{\phi} = 0.01$, $\bar{\phi} = 0.2$ and $\bar{\phi} = 0.4$. Snapshots of the numerical approximation of the density field ϕ are taken at $t = 10$, 30, 50, 1000. The computational domain is $[0, 32]^2$. The parameters are $\epsilon = 0.2$, $M = 1$, $\tilde{\beta} = 0.1$, $T = 1000$. 128^2 Fourier modes are used to discretize the space. The time step is $\delta t = 0.005$

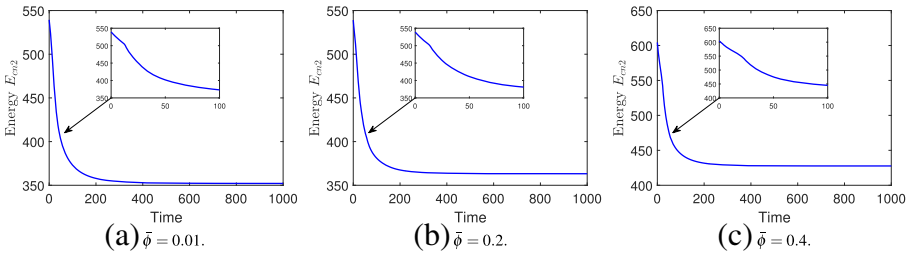

Fig. 6 Evolution of the energy E_{cn2} for phase transition in 2D

$\bar{\phi} = 0.01$, $\bar{\phi} = 0.2$, and $\bar{\phi} = 0.4$. We observe that the energies decrease at all times, which, again, provides numerical evidence for the proposed scheme being unconditionally energy stable.

For 3D simulation, we use 64^3 Fourier modes to discretize the 3D space. The time step is $\delta t = 0.02$. The computational domain is $[0, 50]^3$. The parameters are $\epsilon = 0.56$, $M = 1$, $\tilde{\beta} = 0.1$, and $T = 3000$. Figure 7 presents the steady-state microstructure of the phase transition behavior and Fig. 8 shows the evolution of the energy E_{cn2} with different $\bar{\phi}$. All of the numerical results are consistent with the phase diagram in [3].

5.5 Crystal growth in 2D and 3D

We simulate the crystal growth in a supercooled liquid. For the 2D case, to define the initial configuration inside the computational domain $[0, 800]^2$, we use the following expression to define the crystallites:

$$\phi^0(x_l, y_l) = \bar{\phi} + C\left(\cos(\frac{q}{\sqrt{3}}y_l)\cos(qx_l) - 0.5\cos(\frac{2q}{\sqrt{3}}y_l)\right), \quad l = 1, 2, 3, \quad (5.3)$$

where x_l and y_l define a local system of cartesian coordinates that is oriented with the crystallite lattice, and $\bar{\phi}$, C, and q are constant parameters. We then define the initial configuration by setting three perfect crystallites in three small square patches of the domain. The centers of the three small square patches are located at $(350, 400)$, $(200, 200)$, and $(600, 300)$ and the length of each square is 40. The parameters take the values $\bar{\phi} = 0.285$, $C = 0.446$, and $q = 0.66$. To generate crystallites with different orientations, we define the local coordinates (x_l, y_l) using an affine transformation of the global coordinates (x, y), which produces a rotation given by an angle θ. Also, θ are chosen as $\theta = -\frac{\pi}{4}, 0, \frac{\pi}{4}$, respectively, to generate crystallite lattices with different orientations.

We use 512^2 Fourier modes to discretize the 2D space and use relatively small the time step $\delta t = 0.02$ for better accuracy. The other parameters take the values $\epsilon = 0.25$, $M = 1$, $\beta = 0.9$, and $T = 2000$. Figure 9 shows snapshots of the numerical solution at different times. We observe the growth of the crystalline phase and

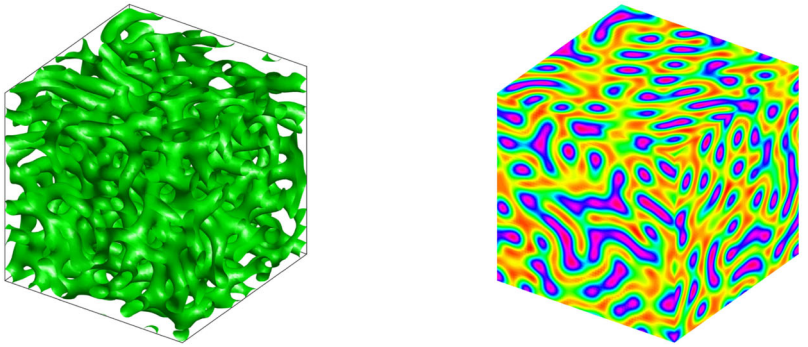

(a) $\bar{\phi} = -0.20$.

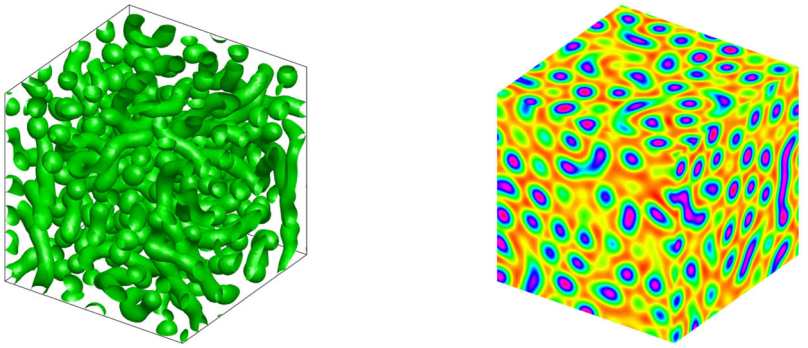

(b) $\bar{\phi} = -0.35$.

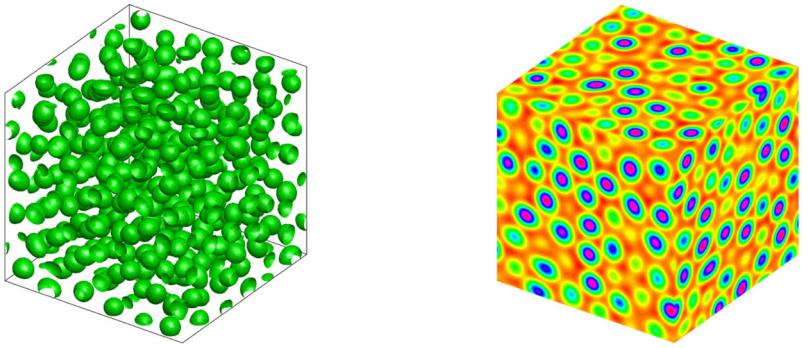

(c) $\bar{\phi} = -0.43$.

Fig. 7 The evolution of the phase transition behavior in 3D with different $\bar{\phi}$. The computational domain is $[0, 50]^3$. The parameters are $\epsilon = 0.56$, $M = 1$, $\tilde{\beta} = 0.1$, and $T = 3000$. 64^3 Fourier modes are used to discretize the space. The time step is $\delta t = 0.02$. Left: isosurface plots of $\phi = 0$. Right: snapshots of the density field ϕ. **a** $\bar{\phi} = -0.20$. **b** $\bar{\phi} = -0.35$. **c** $\bar{\phi} = -0.43$

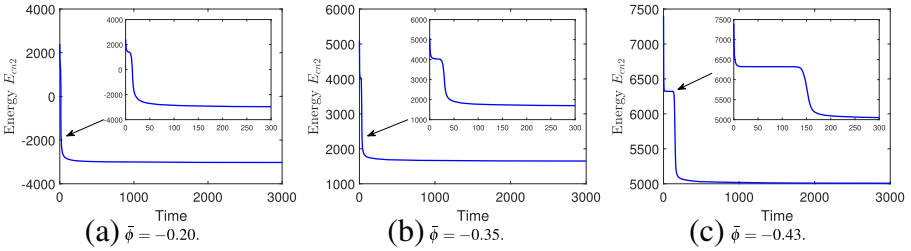

Fig. 8 Evolution of the energy E_{cn2} for phase transition in 3D

the motion of well-defined crystal-liquid interfaces. The different alignment of the crystallites causes defects and dislocations that are clearly observed in the pictures.

For the 3D case, we simulate the growth and interaction of two crystallites inside the computational domain $[0, 100]^3$. An initial condition is generated as follows: $\phi^0 = 0.285 + \text{rand}$, where rand is uniformly distributed random number between -0.01 and 0.01 at the grid points. The other parameters are $\epsilon = 0.25$, $M = 1$,

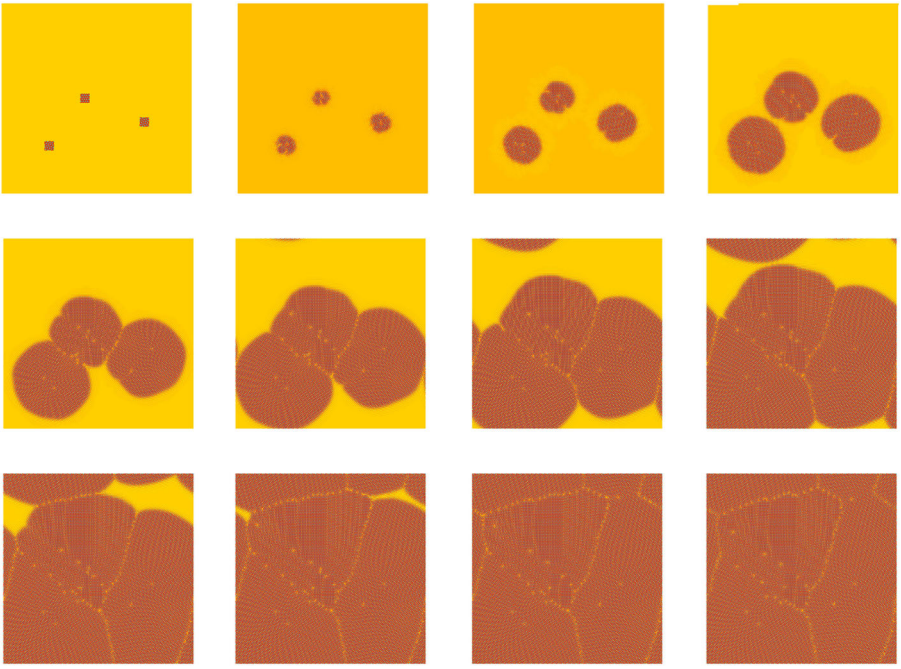

Fig. 9 The 2D dynamical behaviors of the crystal growth in a supercooled liquid. Snapshots of the numerical approximation of the density field ϕ are taken at $t = 0$, 100, 200, 300, 400, 500, 600, 700, 800, 900, 1000, 2000. The computational domain is $[0, 128]^2$. The parameters are $\epsilon = 0.25$, $M = 1$, and $\beta = 0.9$. 128^2 Fourier modes are used to discretize the space. The time step is $\delta t = 0.02$

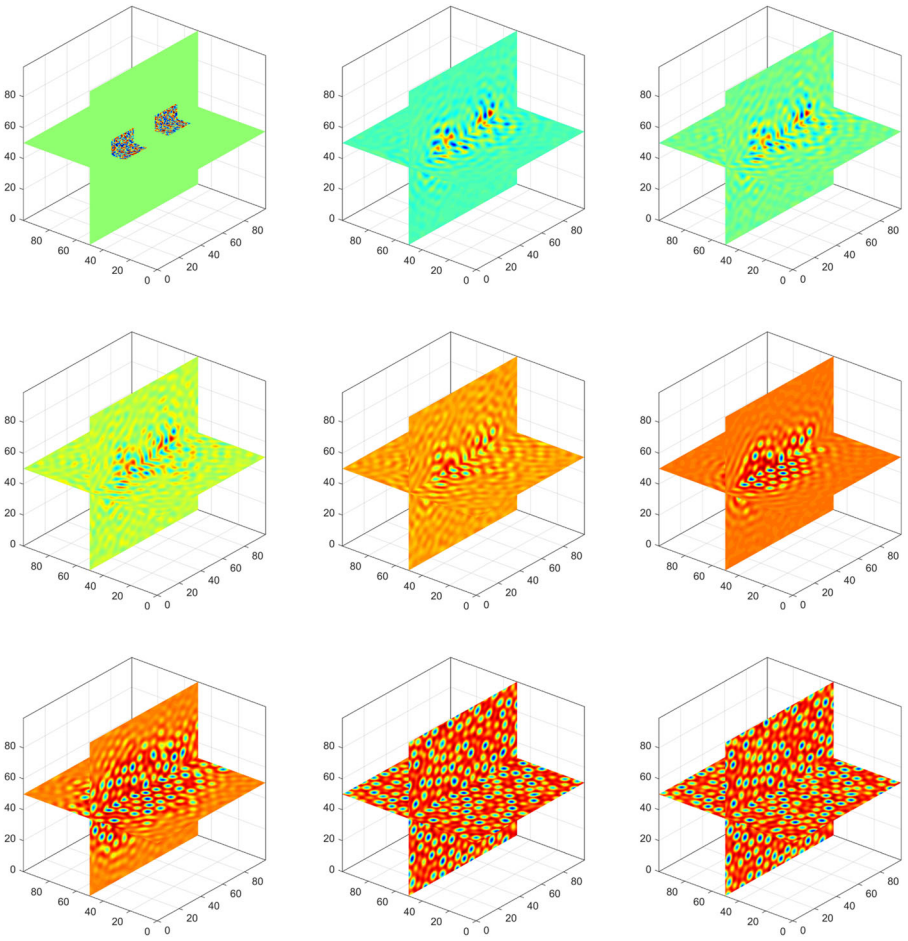

Fig. 10 The 3D dynamical behaviors of the crystal growth in a supercooled liquid. Snapshots of the numerical approximation of the density field ϕ are taken at $t = 0$, 60, 200, 350, 500, 600, 650, 1200, 2000. The computational domain is $[0, 128]^3$. The parameters are $\epsilon = 0.25$, $M = 1$, and $\beta = 0.9$. 128^3 Fourier modes are used to discretize the space. The time step is $\delta t = 0.02$

$\beta = 0.9$, and $T = 2000$. We use 128^3 Fourier modes to discretize the 3D space and the time step $\delta t = 0.02$. In Fig. 10, we observe the growth of the crystalline phase and the motion of crystal-liquid interfaces from the effects of different alignments of crystallites.

Figure 11 shows the evolution of the energy E_{cn2} corresponding to the solution evolution of Fig. 9 in 2D case and Fig. 10 in 3D case, respectively. It is clearly shown that the energy monotonically decays with respect to the time and it means that the numerical result is energy stable.

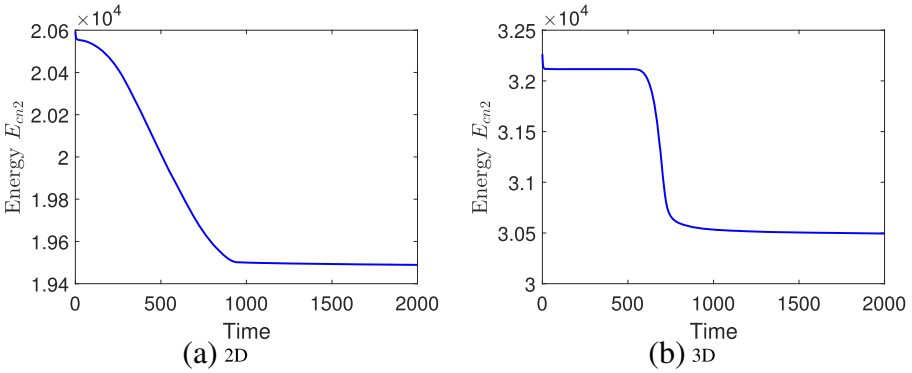

Fig. 11 Evolution of the energy E_{cn2} for crystal growth in a supercooled liquid in 2D and 3D

6 Conclusions

In this paper, we develop three efficient numerical schemes for the MPFC equation, which is a sixth-order nonlinear damped wave equation, by using the novel IEQ approach. Compared to existing nonlinear schemes, the developed schemes can easily conquer the inconvenience from nonlinearities by linearizing the nonlinear cubic term. We show that all the three schemes developed are unconditionally energy stable, and thus allow for large time steps. Moreover, the induced linear system at each time step is proven to be symmetric positive definite so that one can implement the Krylov subspace method with mass lumping as pre-conditioner to solve such system effectively and efficiently. We verify numerically that our schemes are of first- and second-order accuracy in time and present some 2D and 3D numerical results for some benchmark simulations to demonstrate the efficiency and energy stability of the schemes.

Acknowledgments The first author would like to thank Zhen Xu at Beijing Normal University and Yali Gao at Northwestern Polytechnical University for the valuable discussions. The authors also would like to thank the reviewers for their helpful comments and suggestions.

Funding information The work of Q. Li is supported by the China Scholarship Council (CSC No. 201806280137). The work of L. Mei is partially supported by the NSFC under grant no. 11371289. The work of X. Yang is partially supported by the NSF Grant DMS-1720212 and USC ASPIRE I Track-III/IV Fund. The work of Y. Li is partially supported by the NSFC under grant no. 11601416.

References

1. Baskaran, A., Hu, Z., Lowengrub, J.S., Wang, C., Wise, S.M., Zhou, P.: Energy stable and efficient finite-difference nonlinear multigrid schemes for the modified phase field crystal equation. J. Comput. Phys. **250**, 270–292 (2013)

2. Baskaran, A., Lowengrub, J.S., Wang, C., Wise, S.M.: Convergence analysis of a second order convex splitting scheme for the modified phase field crystal equation. SIAM J. Numer. Anal. **51**(5), 2851–2873 (2013)
3. Bueno, J., Starodumov, I., Gomez, H., Galenko, P., Alexandrov, D.: Three dimensional structures predicted by the modified phase field crystal equation. Comput. Mater. Sci. **111**, 310–312 (2016)
4. Chen, L., Zhao, J., Yang, X.: Regularized linear schemes for the molecular beam epitaxy model with slope selection. Appl. Numer. Math. **128**, 139–156 (2018)
5. Chen, R., Yang, X., Zhang, H.: Second order, linear, and unconditionally energy stable schemes for a hydrodynamic model of smectic-A liquid crystals. SIAM J. Sci. Comput. **39**(6), A2808–A2833 (2017)
6. Cheng, Q., Yang, X., Shen, J.: Efficient and accurate numerical schemes for a hydro-dynamically coupled phase field diblock copolymer model. J. Comput. Phys. **341**, 44–60 (2017)
7. Dehghan, M., Mohammadi, V.: The numerical simulation of the phase field crystal (PFC) and modified phase field crystal (MPFC) models via global and local meshless methods. Comput. Methods Appl. Mech. Eng. **298**, 453–484 (2016)
8. Elder, K.R., Grant, M.: Modeling elastic and plastic deformations in nonequilibrium processing using phase field crystals. Phys. Rev. E **70**(051), 605 (2004)
9. Elder, K.R., Katakowski, M., Haataja, M., Grant, M.: Modeling elasticity in crystal growth. Phys. Rev. Lett. **88**(245), 701 (2002)
10. Elder, K.R., Provatas, N., Berry, J., Stefanovic, P., Grant, M.: Phase-field crystal modeling and classical density functional theory of freezing. Phys. Rev. B **75**(064), 107 (2007)
11. Galenko, P.K., Gomez, H., Kropotin, N.V., Elder, K.R.: Unconditionally stable method and numerical solution of the hyperbolic phase-field crystal equation. Phys. Rev. E **88**(013), 310 (2013)
12. Gong, Y., Zhao, J., Wang, Q.: Linear second order in time energy stable schemes for hydrodynamic models of binary mixtures based on a spatially pseudospectral approximation. Adv. Comput. Math. **44**(5), 1573–1600 (2018)
13. Gong, Y., Zhao, J., Wang, Q.: Second order fully discrete energy stable methods on staggered grids for hydrodynamic phase field models of binary viscous fluids. SIAM J. Sci. Comput. **40**(2), B528–B553 (2018)
14. Gong, Y., Zhao, J., Yang, X., Wang, Q.: Fully discrete second-order linear schemes for hydrodynamic phase field models of binary viscous fluid flows with variable densities. SIAM J. Sci. Comput. **40**(1), B138–B167 (2018)
15. Grasselli, M., Pierre, M.: Energy stable and convergent finite element schemes for the modified phase field crystal equation. ESAIM Math. Model. Numer. Anal. **50**(5), 1523–1560 (2016)
16. Guo, R., Xu, Y.: A high order adaptive time-stepping strategy and local discontinuous Galerkin method for the modified phase field crystal equation. Commun. Comput. Phys. **24**(1), 123–151 (2018)
17. Lee, H.G., Shin, J., Lee, J.Y.: First- and second-order energy stable methods for the modified phase field crystal equation. Comput. Methods Appl. Mech. Eng. **321**, 1–17 (2017)
18. Li, H., Ju, L., Zhang, C., Peng, Q.: Unconditionally energy stable linear schemes for the diffuse interface model with Peng-Robinson equation of state. J. Sci. Comput. **75**(2), 993–1015 (2018)
19. Provatas, N., Dantzig, J., Athreya, B., Chan, P., Stefanovic, P., Goldenfeld, N., Elder, K.: Using the phase-field crystal method in the multi-scale modeling of microstructure evolution. JOM **59**(7), 83–90 (2007)
20. Shen, J., Yang, X.: Numerical approximations of Allen-Cahn and Cahn-Hilliard equations. Discrete Contin. Dyn. Syst. **28**(4), 1669–1691 (2010)
21. Shen, J., Yang, X.: A phase-field model and its numerical approximation for two-phase incompressible flows with different densities and viscosities. SIAM J. Sci. Comput. **32**(3), 1159–1179 (2010)
22. Stefanovic, P., Haataja, M., Provatas, N.: Phase-field crystals with elastic interactions. Phys. Rev. Lett. **96**(225), 504 (2006)
23. Stefanovic, P., Haataja, M., Provatas, N.: Phase field crystal study of deformation and plasticity in nanocrystalline materials. Phys. Rev. E **80**(046), 107 (2009)
24. Swift, J., Hohenberg, P.C.: Hydrodynamic fluctuations at the convective instability. Phys. Rev. A **15**, 319–328 (1977)
25. Wang, C., Wise, S.M.: An energy stable and convergent finite-difference scheme for the modified phase field crystal equation. SIAM J. Numer. Anal. **49**(3), 945–969 (2011)
26. Yang, X.: Error analysis of stabilized semi-implicit method of Allen-Cahn equation. Discrete Contin. Dyn. Syst. Ser. B **11**(4), 1057–1070 (2009)

27. Yang, X.: Linear, first and second-order, unconditionally energy stable numerical schemes for the phase field model of homopolymer blends. J. Comput. Phys. **327**, 294–316 (2016)
28. Yang, X.: Numerical approximations for the Cahn-Hilliard phase field model of the binary fluid-surfactant system. J. Sci. Comput. **74**(3), 1533–1553 (2018)
29. Yang, X., Ju, L.: Efficient linear schemes with unconditional energy stability for the phase field elastic bending energy model. Comput. Methods Appl. Mech. Eng. **315**, 691–712 (2017)
30. Yang, X., Zhao, J., He, X.: Linear, second order and unconditionally energy stable schemes for the viscous Cahn-Hilliard equation with hyperbolic relaxation using the invariant energy quadratization method. J. Comput. Appl. Math. **343**, 80–97 (2018)
31. Yang, X., Zhao, J., Wang, Q.: Numerical approximations for the molecular beam epitaxial growth model based on the invariant energy quadratization method. J. Comput. Phys. **333**, 104–127 (2017)
32. Yang, X., Zhao, J., Wang, Q., Shen, J.: Numerical approximations for a three-component Cahn-Hilliard phase-field model based on the invariant energy quadratization method. Math. Models Methods Appl. Sci. **27**(11), 1993–2030 (2017)
33. Zhao, J., Wang, Q., Yang, X.: Numerical approximations for a phase field dendritic crystal growth model based on the invariant energy quadratization approach. Internat. J. Numer. Methods Eng. **110**(3), 279–300 (2017)
34. Zhao, J., Yang, X., Gong, Y., Wang, Q.: A novel linear second order unconditionally energy stable scheme for a hydrodynamic **Q**-tensor model of liquid crystals. Comput. Methods Appl. Mech. Eng. **318**, 803–825 (2017)